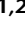# Characterizing the three-dimensional distribution of schooling reef fish with a portable multibeam echosounder

Matthew M. Holland [1,2]*** **Alistair Becker** [3] **James A. Smith** [1,4] **Jason D. Everett** [1,5] **Iain M. Suthers** [1,2]

[1]Evolution and Ecology Research Centre, School of Biological, Earth and Environmental Sciences, University of New South Wales, Sydney, New South Wales, Australia
[2]Sydney Institute of Marine Science, Mosman, New South Wales, Australia
[3]New South Wales Department of Primary Industries, Port Stephens Fisheries Institute, Taylors Beach, New South Wales, Australia
[4]Institute of Marine Sciences, University of California Santa Cruz, Santa Cruz, California
[5]Centre for Applications in Natural Resource Mathematics, School of Mathematics and Physics, The University of Queensland, St Lucia, Queensland, Australia

Abstract

Multispecies schools of small planktivorous fishes are important constituents of reefs and coastal infrastructure; however, determining the extent and distribution of these schools is challenging. Here, we describe a novel use of a low-cost portable multibeam echosounder from a small vessel, which can concurrently measure detailed bathymetry and the distribution of mid-water targets with high spatial accuracy, regardless of light availability or water clarity. Fish abundance and biomass are not easily quantified by multibeam echosounders, so we developed a new metric for delineating the gridded horizontal distribution of school thickness, and assessed the metric's efficacy by examining its correlation with mean volume backscattering strength derived from a calibrated 38 kHz split-beam echosounder ($R = 0.67$). We measured the distribution of fish school thickness around clusters of large concrete modules of an artificial reef using a multibeam echosounder, complemented with underwater video to aid species identification. The mean distribution of school thickness was mapped around the reef field with generalized additive mixed models. Model spatial predictions indicated schools aggregated around module clusters, rather than individual modules. Dynamic schools of fish in relatively shallow coastal waters (~ 30 m) can be surveyed over 400,000 m^2 at 3 m s^{-1} in just 60 min. Portable multibeam echosounders are an accessible and valuable addition to quantifying the dynamic distributions of coastal fishes around features with high vertical relief.

Littoral marine ecosystems are characterized by diverse and abundant fish communities, particularly around reefs and areas of high structural complexity (Hunter and Sayer 2009; Graham and Nash 2013; Parsons et al. 2016; Holland et al. 2020). Fish display a diversity of habitat associations in these environments, with varying use of the water column and benthic environment. Measuring the fine-scale distribution of fishes is valuable for a better understanding of coastal ecosystems, because distribution can indicate essential habitats, trophic processes such as predation and plankton depletion, and the contribution of natural and artificial habitats to fish production and fishery enhancement (Hamner et al. 1988; Claisse

et al. 2014; Champion et al. 2015; Smith et al. 2016). Some of the most abundant structure-associated fishes in the littoral zone are zooplanktivores (Truong et al. 2017; Morais and Bellwood 2019), but their fine-scale habitat use is difficult to assess, due to the often broad use of the surrounding water column to school and forage (Bellwood et al. 2019).

Several studies have modeled the horizontal distribution of fish around artificial structures by saturating the reef field with stationary underwater video (Scott et al. 2015; Smith et al. 2017; Becker et al. 2019), while others have investigated vertical distribution with underwater visual census (Rilov and Ben-ayahu 1998) and camera-mounted remotely operated vehicles (McLean et al. 2019), but measuring three-dimensional distribution remains a challenge. While these visual techniques do provide valuable species-composition data (dos Santos et al. 2010; Scott et al. 2015; Smith et al. 2017; Becker et al. 2019), they are not well suited for studying the distribution of

*Correspondence: m.holland@unsw.edu.au

Table 1. Glossary of terms.

Fisheries acoustics	A field of research which uses active acoustic instruments (echosounders) to measure the distribution of marine organisms with reflected sound waves (Simmonds and MacLennan 2013)
Echosounder	An instrument which generates and detects reflected sound waves to measure physical and/or biological underwater objects, including the seafloor, fish, plankton, aquatic vegetation, and the separation of water masses
Split-beam echosounder	Instrument emitting a single beam which is then received on three or more sectors of the transducer to measure phase differences and determine position of targets relative to beam Centre. This information is used to compensate target strength measurements for off-axis targets.
Multibeam echosounder (MBES)	Instrument containing potentially hundreds of beams, which are divided using a technique known as beamforming, which allows for the directional partitioning of the transmitted and received acoustic energy through the constructive and destructive interference of sound waves
Frequency (kHz)	The number of cycles (in thousand cycles per second) that an acoustic wave repeats itself (e.g., 38 kHz is a standard frequency for detecting swim-bladdered fish with split-beam transducers)
Calibration	Correcting the drift in sensitivity experienced over time by acoustic instruments by placing a metal sphere with precise acoustic properties within the beam and adjusting the receiver parameters to register a known value
Mean volume backscattering strength (MVBS) in dB re 1 m^{-1}	A measure of the acoustic energy reflected by targets, averaged over a finite volume

schooling fishes like zooplanktivores, which can aggregate over large volumes not easily surveyed in one dimension.

These methods all suffer from inherent biases and limitations. With underwater visual census, certain taxa are prone to be attracted to or repelled by divers (MacNeil et al. 2008; Dickens et al. 2011). Divers can also introduce error through visual estimation of size and abundance (Edgar et al. 2004; Harvey et al. 2004). Further, diver surveys are limited by light availability, water clarity, depth, and bottom time (Watson et al. 2005). Many of these factors are also valid concerns associated with video methods, also affected by double-counting of individual fish (Denney et al. 2017). For applications involving highly abundant, densely packed schooling fish it is very difficult to accurately estimate abundance due to the limited range and field of view associated with both diver and

remote video methods (Murphy and Jenkins 2010). Under these circumstances, fisheries acoustics techniques have often proved valuable.

Acoustic methods have been extensively applied to monitoring the regional distribution of small schooling fishes—typically forage fish such as herring and sardines—which often form large single-species schools in low-diversity pelagic environments (O'Donnell et al. 2019; Kuriyama et al. 2020). Echosounders have also been used measure fish distributions around structures, such as shipwrecks (Paxton et al. 2019), artificial reefs (Lee 2013), and oil and gas extraction infrastructure (Soldal et al. 2002; Punzo et al. 2015). Most modern scientific echosounders operate using split-beam transducers (Table 1), with a narrow beam (typically <15°; Taylor and Ebert 2012) to resolve a detailed volume-adjusted two-dimensional profile of the water column in the along-track direction (Rudstam et al. 1999). Backscatter values (Table 1) obtained from these instruments can be calibrated using metal spheres of precise diameter and acoustic properties (Foote and MacLennan 1984). These instruments have high spatial resolution along the vessel track; however, the fine-scale spatial distribution of fish and bathymetry in the across-track direction cannot be resolved. Thus, school shape, size, and volume are difficult to determine as it is unknown whether the vessel intersected the center or edge of a school (Kieser et al. 1993). Similarly, the distribution of schools relative to fine scale variations in bathymetry is only detectable along the vessel track.

The precise ranging capabilities and large swath coverage of multibeam echosounders make them better suited to approaching this problem. Multibeam echosounders (MBES) operate with much larger swath width (typically 120–150°; Colbo et al. 2014). Unlike traditional echosounders, MBES use a technique known as beamforming, which allows for the directional partitioning of the transmitted and received acoustic energy through the constructive and destructive interference of sound waves (Jung et al. 2018). This enables the across-track dimension to be divided up into hundreds of separate beams, facilitating the resolution of spatial features in the direction perpendicular to the vessel track. In this way, MBES record data in both the along-track and across-track directions, providing a means for generating detailed three-dimensional output.

Recently a range of more affordable portable MBES have been introduced, which are marketed toward high-end recreational boat owners, commercial fishers, and researchers operating smaller, shared-use trailer vessels for applications in shallow water and coastal areas. In relatively shallow depths (20–100 m), these modern MBES can efficiently survey large areas of seafloor and the lower water column. The high number of narrow beams, and integrated real-time compensation for pitch, heave, roll and tidal height allow MBES to measure the georeferenced position of targets, with horizontal and vertical accuracies generally less than 5 cm at ranges under 15 m (Dix et al. 2012).

MBES generate significant data, in the order of gigabytes per minute, presenting challenges for researchers in terms of processing and storage (Colbo et al. 2014). Due to the immense quantity of data generated, the ability of MBES to retain water column data, in addition to seafloor data, has only been possible since the late 1990s (Mayer et al. 2002). Many modern MBES still do not allow for logging of water column data (Colbo et al. 2014). MBES data often requires considerable aggregation, or reduction in dimensionality and/or resolution, in order to be used practically for statistical modeling approaches with traditional computer hardware (Colbo et al. 2014). Another drawback is the technical difficulty of calibration (Foote et al. 2005) which typically requires gain adjustment parameters to be measured for each beam independently (Trenkel et al. 2008). For an instrument with potentially hundreds of beams, this is impracticable for many users and as a result many consumer-grade (rather than scientific-grade) MBES cannot be user-calibrated. While most MBES are calibrated initially by the manufacturer, they have a tendency to drift in sensitivity over time (Roche et al. 2018). Further, unlike the narrow vertically oriented beam of split-beam echosounders, MBES detect targets which are not orthogonal to the transmitted pulse, adding additional uncertainty to target strength measurements (Colbo et al. 2014). A major consequence of these two issues is that backscatter values generated from consumer-grade MBES cannot be reliably used to derive fish abundance or biomass.

The comparatively low price-tag (relative to scientific-grade echosounders), portability, and user-friendly interface associated with many of the newer consumer-grade MBES may appeal to marine ecologists who may not have the technical skills of acousticians. They can provide quantitative data pertaining to the spatial distribution and behavior of schooling fish, for such applications as: monitoring the successional establishment of schooling fish at newly deployed artificial structures (Leitao et al. 2008; Folpp et al. 2011; Lowry et al. 2014); examining the distribution and behavior of schooling fish at night (Rieucau et al. 2015; Becker et al. 2016); and recording the distribution of schools concurrent with benthic habitat classification (Monk et al. 2010; Monk et al. 2012). In short, MBES offer superior technology for measuring the three-dimensional distribution of schooling reef-associated and near-shore fishes. However, due to the complexities associated with deriving estimates of abundance or biomass from MBES, it remains challenging to quantify the fine-scale distribution of schools in these environments.

Here, we demonstrate a simple and computationally efficient method for defining the distribution of fish schools from MBES water column data in relatively shallow coastal areas. We apply a similar approach to that which is used to generate bathymetric surfaces from MBES point clouds. We extract three-dimensional georeferenced samples and project them onto a two-dimensional grid by calculating a mean value for each grid cell. This results in a spatial variable representing the thickness of a school for any given point in two dimensions, which could be used as an index of distribution for schooling fish.

We chose to evaluate school thickness, rather than mean volume backscatter, for several reasons. Due to the outer beams intersecting targets nonorthogonal to the transmitted pulse, target strength for an identical target can vary depending on where in the swath it is detected. By identifying abrupt transitions in backscatter strength across the vertical plane, we can overcome this bias by delineating the spatial boundaries of schools, rather than integrating the acoustic energy contained within them (Zwolinski et al. 2009). A key attribute of this "school thickness" approach is that it can be used to map the distribution of multispecies fish schools in shallow water from small vessels within proximity of the seafloor. This method is robust to spikes attributed to noise because it involves no echo integration, and such outliers contribute little to the larger spatial patterns. School thickness can also be derived from instruments that cannot be user-calibrated, so long as the GPS antenna, motion adjustments, and range estimation are accurate.

The overall goal of this article is to present a convenient methodology for marine ecologists to use MBES to map the three-dimensional distribution of schooling fish in relation to shallow coastal features. We have two main aims: (1) to validate our approach by comparing two methods for calculating "school thickness" with backscatter from a calibrated split-beam echosounder; and (2) demonstrate a practical application of the "school thickness" method using a portable MBES and generalized additive mixed models (GAMMs) to map the distribution of schooling fish around an artificial reef.

Materials and procedures

Site description

For both the split-beam validation and the MBES practical application, we surveyed a set of artificial reef modules, 900 m off the coast of Sydney, Australia (34.0943°S 151.1776°E). The reefs were deployed in 30 m water over an area of bare sand in 2017 to enhance recreational fisheries. Each concrete module weighs 25 t and stands 5 m high, with a footprint of 4 × 4 m. Modules are deployed in five clusters of 3–4 modules, with one module in each cluster supporting a 4 m steel tower. Artificial reefs such as these typically host isolated, compact and discrete epi-benthic schools (Becker et al. 2019) which facilitate the resolution of individual schools with MBES.

Species composition from remote video

We used remote video to identify the fish species present in each survey. MBES are only suitable for identifying species of schooling fish when there is some prior knowledge or in situ validation of taxa-specific school characteristics (Guillard et al. 2011; Innangi et al. 2016). Therefore, to identify the dominant species present, we deployed a single remote camera

deployment per survey at the center of the reef complex for 30 min. We generated a relative proportion of abundance, by subsampling each video with five random 2-min intervals (Basford et al. 2016) and calculating the mean of the proportionate abundance, from MaxN, for each taxon across surveys (Ellis and DeMartini 1995). In this case, MaxN was the maximum abundance of each species visible within a single frame within each sampling interval. We used underwater video primarily to complement MBES and enable species identification.

Multibeam acoustic data collection

We conducted five MBES surveys at the Sydney artificial reef approximately 3 h after sunrise (14 August, 03 September, 26 September, 31 October, and 08 November 2019) using a WASSP WMB-1320Fi portable 160 kHz multibeam echosounder (WASSP Limited, Auckland, New Zealand). The vessel was a 14 m long, charter fishing boat constructed of wood. The transducer was mounted over the gunwale on a custom-built aluminum pole assembly, which was stabilized by steel cables under high tension and suspended 1.5 m below the surface. This MBES has a chirp range of 130–190 kHz and a maximum range resolution of 2 cm. The MBES was calibrated by the manufacturer to be within 3 dB of the nominal model at 160 kHz. Acquisition range was set to 50 m, with transmission power of 36 W and variable pulse duration and frequency. Acoustic energy of 160 kHz travels through seawater with a wavelength of < 1 cm, which is substantially smaller than any individual fish we wished to measure. The transducer assembly was fitted with an integrated Hemisphere Vector V103

Smart Antenna (Hemisphere GNSS, Scottsdale, U.S.A.) which adjusts for pitch, heave and roll in real-time and has a positioning accuracy of ∼ 2 cm under ideal conditions. The recording software also compensated for tidal height in real-time using a predictive tide model. The seafloor of artificial reef field was completely ensonified with six evenly spaced parallel transects. Each subsequent transect was designed to have 50% overlap with the previous transect at the seafloor.

Multibeam acoustic data processing

All acoustic data were processed using Echoview v9.0 (Echoview Software Pty Ltd, Hobart, Australia), although other hydroacoustic analysis software would also be suitable (e.g., QPS Qimera). Associated Echoview files and R-scripts for a working example are available from: https://github.com/hollam2/WASSP_methods.

After data were imported into Echoview, the first processing step involved isolating fish schools from noise and bottom backscatter (Fig. 1). Initially we excluded some of the outer beams, due to their tendency to produce erroneous measurements (Step M1; Fig. 1), caused by their oblique angle of intersection with the seafloor (Colbo et al. 2014). We then conducted an XYZ convolution to blur the acoustic data (Step M2) (Kang 2011) and generated a bathymetry surface from the same data, using Echoview's built-in algorithm (Step M3).

This surface was exported (Step M4) and modified in R v3.6.3 (R Core Team 2018) to incorporate the three-dimensional outlines of artificial structures (Step M5), such as the concrete artificial reef modules, as these hollow objects are
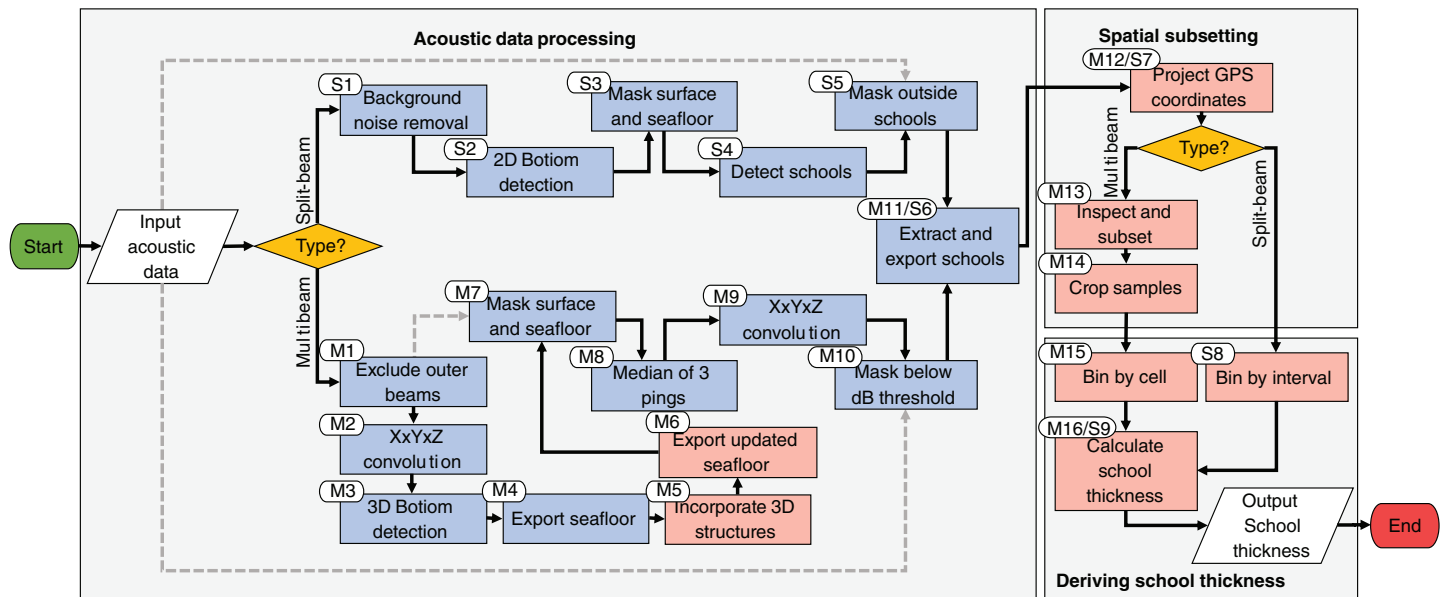

Fig 1. Flowchart outlining the method for processing acoustic data from both split-beam and MBES to produce the "school thickness" variable. Procedures which are carried out in Echoview are represented in blue, while procedures in R are represented in pink. Dashed gray lines indicate the incorporation of unaltered data from a previous step to be extracted with a Boolean mask. The major parts of the process are categorized and labeled with the three gray boxes in background. Process steps are numbered in sequence and labeled according to whether they pertain to split-beam (prefix: S) or multibeam (prefix: M).
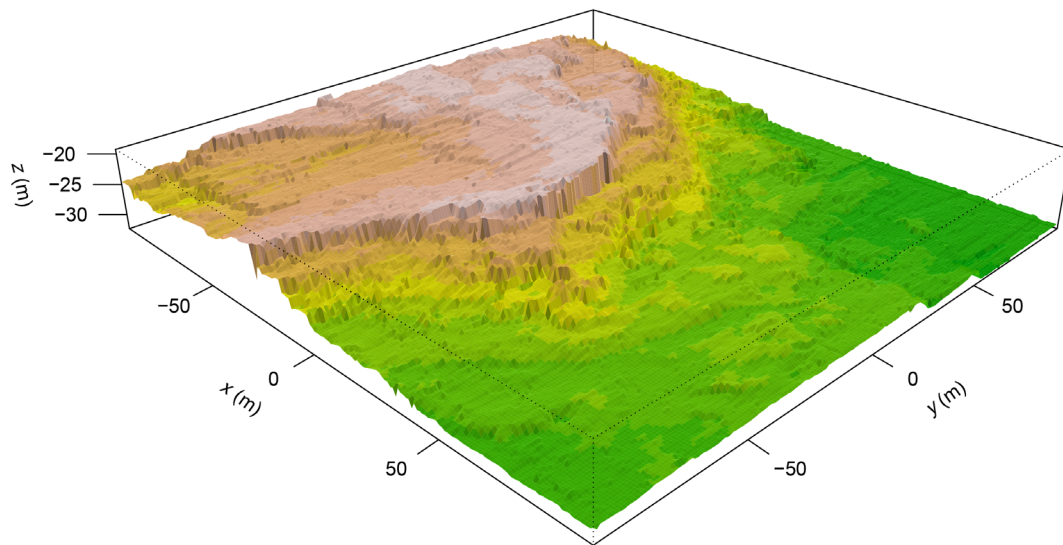
Fig 2. One-meter resolution digital elevation model for a natural reef site generated from data collected with the WASSP MBES. Note the z-axis has a 3× exaggeration to highlight variations in bathymetry.

not readily detected by the algorithm for bathymetry detection. This additional step was unnecessary for natural reef sites, as the MBES generally performed well at detecting natural seafloor variation (Fig. 2). The bathymetry surface was then offset by 1 m to provide a small buffer for manually rendered structures and seafloor detection anomalies (Ona and Mitson 1996) and was subsequently imported back into Echoview (Step M6) so that seafloor and surface data could be masked out (Step M7). It is important to note that due to the high level of accuracy required for this bathymetry surface, it should ideally be generated from this concurrent MBES data, rather than relying on archival data, as the interaction of currents and benthic organisms with artificial reef structures can gradually alter seafloor morphology (Tassetti et al. 2015) and reef structures may shift and deteriorate over time (Sala et al. 2007).

After the masking step, we calculated the median value for every three pings in sequence to smooth the data (Step M8) and finally applied an additional XYZ convolution with a top-hat transformation (Dougherty 1992) to facilitate feature extraction (Step M9). This data were then subset with a user-specified threshold value, in our case −65 dB, to create a three-dimensional Boolean mask, which was then applied to the original unaltered data to exclude volume most likely to be noise and extract samples most likely to contain schools (Step M10). The combination of these processing steps essentially detects and refines the major transitions in mid-water acoustic energy across space that define the face around schools.

Spatial subsetting

Extracted georeferenced samples were exported from Echoview as three column XYZ data (Step M11). To keep file size to a minimum, empty volumes without target detections were not exported. All subsequent analyses were conducted using R (R Core Team 2018). Samples and bathymetry were projected into a UTM coordinate system (Step M12) and plotted in three dimensions and visually inspected (Step M13) using the RGL package (Murdoch 2001). This package can be used to generate detailed interactive three-dimensional visualizations which can be exported to html and viewed in a web browser (Fig. 3).

Upon plotting, any visually apparent noise spikes (sometimes caused by bubbles) which were not suitably removed by the previous steps were then excluded by manually defining the three-dimensional extent of rectangular prisms to exclude erroneous samples. This step was rarely required as the previous processing steps were generally effective at isolating schools from noise. In addition, any erroneous below-bottom samples were also excluded during this step by using the bathymetry surface generated in step M5.

For all types of echosounders, comparing targets at different depths is complicated by the fan shape of the acoustic beam. Based on the shape of the beam, with the transducer deployed facing directly downward, it is generally more effective detecting benthic targets than those in the upper water column, where the beam is much narrower. This is particularly evident when using MBES due to their considerably large swath width. Additionally, the characteristic tendency for MBES to produce arc-shaped noise artifacts (across-track), caused by interference from sidelobes, reduces the usability of data from the outer beams near to the seafloor (Clarke 2006). However, as the wide swath angle used by MBES generates a large ensonified volume, it is possible to eliminate some data to reduce this bias and interference while retaining enough data to still take advantage of the wider swath.
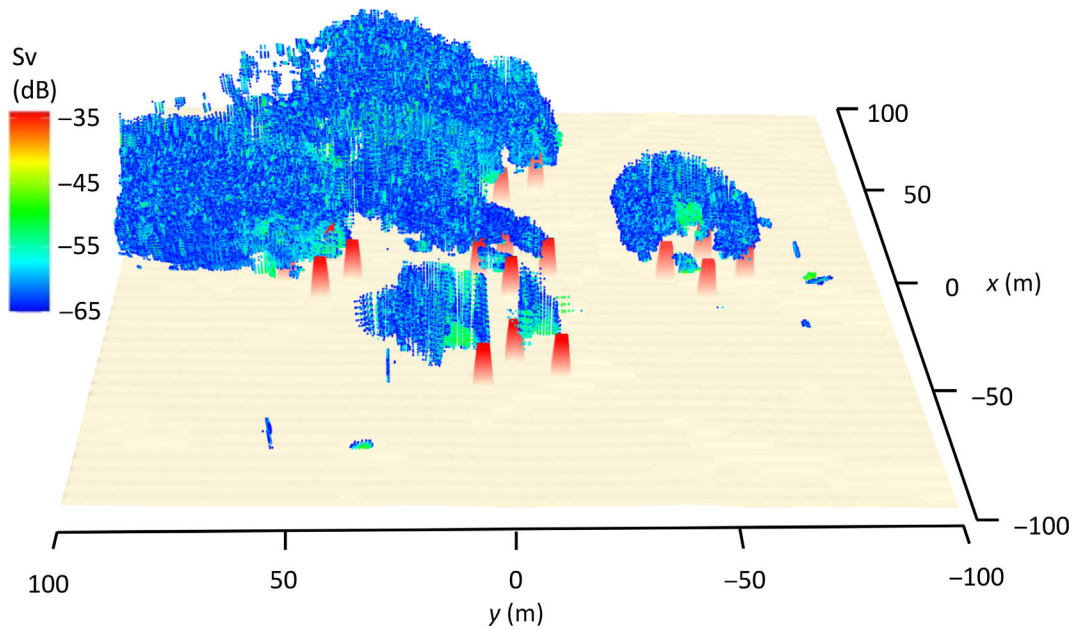
Fig 3. Raw three-dimensional (3D) spatially referenced samples from one survey of the artificial reef, colored by mean volume backscatter (Sv). Bathymetry surface is also shown and has been modified to accommodate the shapes of artificial reef modules, in red.
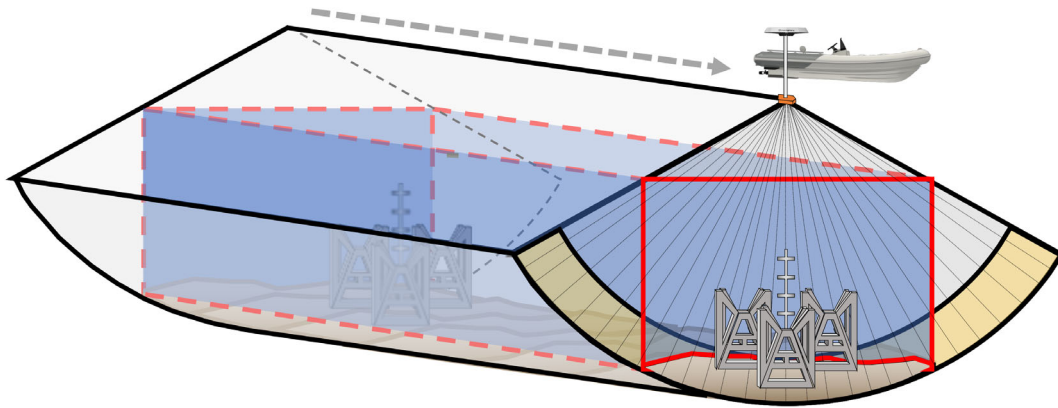

Fig 4. Swath (light gray) conversion to rectangular prism (blue and outlined in red) with variable width, through limiting the extent of acoustic data in the across-track direction and setting a minimum depth threshold. The red polygon below the survey vessel outlines the profile of the 3D shape used to subset the acoustic data spatially. This effectively excludes most of the swath likely to be affected by sidelobe artifacts (yellow) in the outer beams where they intersect the seafloor. Note, beams are included to aid visualization and do not correspond to the number of beams used in this study.

To alleviate this disparity in detectability and to differentiate between surveyed and unsurveyed area, samples were cropped to effectively modify the swath so that detectability remained more consistent throughout (Step M14). Further, this step virtually eliminated spurious side lobe seafloor detections, which tend to be stochastic due to the scattering effects of beams intersecting seafloor objects at oblique angles (Colbo et al. 2014). Data were initially subset to exclude samples occurring shallower than a user-specified depth, effectively cropping the beam pattern. This step was made possible by the motion compensation adjustments provided by the Hemisphere Smart Antenna. The width of the swath at this specified depth was then calculated using trigonometry by using the swath width (120° in our case) and minimum depth (10 m in our case). A polygon was then generated, consisting of the union of circular buffers calculated from the GPS-detected coordinates along the vessel track, with radii equivalent to the swath widths calculated in the previous step. This polygon was used to crop the edges of the swath. This process cropped the top and sides of a triangular
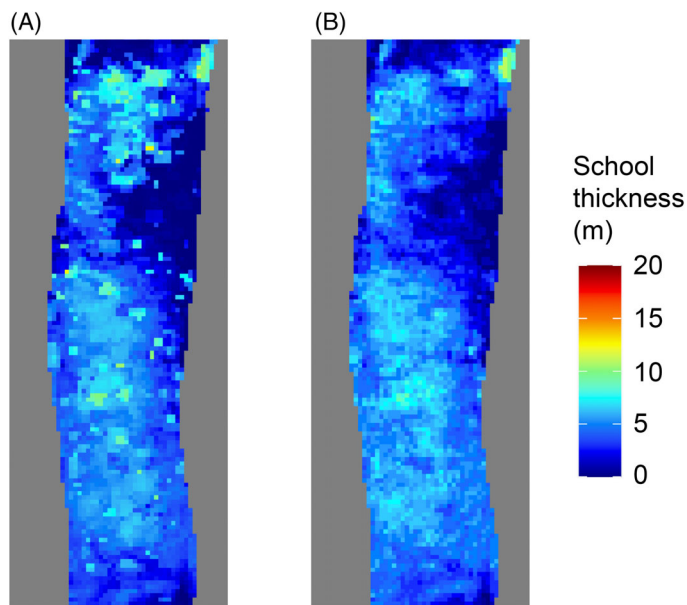
Fig 5. Gridded school thickness outputs comparing the difference method (**a**) and the sum method (**b**). Note the isolated high values on (**a**) which are not present in (**b**), resulting from lone targets or small schools overlapping with schools near the seafloor.

prism to transform it into an internal rectangular prism with varying maximum depth and more consistent detectability throughout its vertical and horizontal extents (Fig. 4). Even with this cropping, a vessel traveling 3 m s^{-1} in 30 m water depth could survey 400,000 m^2 of seafloor and adjacent water column in only 1 h.

Deriving school thickness

To derive a metric for school thickness (a measure of a fish school's vertical extent), two methods were explored and compared using the same data set. Both methods involved initially binning data into 1 m x and y horizontal intervals, creating a topographic grid (Step M15).

The first method, referred to hereafter as the "difference method," involved calculating the minimum and maximum depth of all samples occurring within each cell of the grid and calculating the difference between these two values to derive a measure of school thickness (Step M16). One drawback of this method is the potential to produce artificially inflated values when a lone fish or school higher in the water column overlaps with a school lower in the water column. This method presumes that the empty water between the highest and lowest occurring samples contains fish and would thus create artificially inflated values for such cases of overlap. Furthermore, as schools increase in size, individual fish are less aware of the overall distribution of their school and must base their movements and behavior on that of their more immediate neighbors (Paramo et al. 2007). As a result, large schools tend to exhibit more heterogeneous density throughout their volume,

and are composed of a complex arrangement of high density volumes or nuclei, and empty or low density volumes, also known as vacuoles (Guillard et al. 2011).

We tested a second method to exclude these empty volumes, referred to hereafter as the "sum method." This involved an additional step, which binned samples into depth layers of 1 m thickness (Step M16). For each grid cell, the number of layers containing at least one target detection were summed. If a grid cell contained fish in every layer, then the calculated school thickness derived using the sum method and the difference method would be equivalent. The sum method should be more robust to the presence of vacuoles (Fréon et al. 1992; Paramo et al. 2007; Guillard et al. 2011), spatially overlapping schools or lone targets overlying schools (Fig. 5). In such cases, lone targets would only contribute an additional 1 m to school thickness over a single cell (assuming the target is < 1 m in all dimensions) and overlapping schools would still represent a proxy for the total abundance occurring in each cell. In cases where it is desirable to differentiate between targets occurring in different sections of the water column, georeferenced samples could be sectioned by depth and school thickness could be calculated for each slice of water column independently.

The use of 1 m resolution layers to derive school thickness from the sum method is arbitrary and it is possible to modify the vertical resolution for other applications depending on the range resolution of the MBES; however, for the sake of simplicity, we maintained the same resolution in all three dimensions.

Modeling school distribution around an artificial reef

School thickness is a variable which can be applied to resolve patterns in how fish use the space within their environment. It can resolve with very high spatial accuracy where fish typically aggregate in high volumes and where fish are typically absent and may provide insight (and supplement existing visual methods) for research on reef function (Champion et al. 2015; Truong et al. 2017) and artificial reef habitat value (Smith et al. 2016; Egerton et al. 2021). School thickness is mapped in each survey and is thus represented by the raw data. Modeling this raw data allows us to explore important correlates (like distance to structure) and efficiently estimate the mean distribution and thickness from multiple surveys.

To examine whether there were consistent patterns in the mean distribution of school thickness around the artificial reef across multiple surveys, school thickness from each MBES survey was processed into a raster grid, on a transect-by-transect basis, with the previously described sum method using the "rasterize" function from the Raster package (Hijmans et al. 2015) in R (Supporting Information Fig. S1). The combined extent of grids was cropped to fit a 300 m square positioned over the reef centroid (dos Santos et al. 2010). Grids were aggregated to 5 m resolution to improve the

computational efficiency of model fitting. Aggregation was conducted by calculating the mean value for school thickness for each grid cell within each transect ($n = 9034$).

To model the mean spatial distribution of school thickness around the reef, we created a GAMM that used orthogonal coordinates as predictors:

$$\text{Thickness} \sim s(x,y) + 1 \,|\, \text{date}$$

where the variable $s(x,y)$ is a two-dimensional product smoother of grid cell coordinates to resolve the spatial distribution of school thickness in both horizontal directions (x and y). We also included survey "date" as a random factor to account for day-to-day variation. We assessed several values for the k-parameter for the smooth term (5, 10, 25, 50, 75, 100; *see* Supporting Information Fig. S2); however, we chose to use $k = 50$ to resolve spatial patterns in the data without overfitting. Several studies have found that fish abundance drops off rapidly after 30–50 m (Boswell et al. 2010; dos Santos et al. 2010; Scott et al. 2015; Smith et al. 2017; Becker et al. 2019). To determine the spatial extent to limit our model, we created a binomial GAMM with logit-link to predict probability of target occurrence, with a smoother of "distance from the nearest module" as the only predictor and date as a random effect. Model predictions indicated probability of target occurrence leveled off at $\sim 20\%$ at distances beyond 70 m (Supporting Information Fig. S3). Thus, it was appropriate to restrict the spatial extent to 70 m from the nearest module to model school thickness. We chose a Tweedie distribution with log-link to model continuous positive values with zero inflation. We refer to this model hereafter as our "school thickness distribution model."

We chose to use this model structure over that used in Becker et al. (2019) because it led to better performance and was more generalizable. The advantage of this model structure is that it creates a flexible surface, which can be compared to the distribution of spatial features (such as artificial reefs) to examine their influence on the distribution of school thickness. School thickness is visualized in two dimensions and is a depth-aggregated proxy used to represent fish abundance. One caveat to this approach is that it averages over what are likely important drivers of distribution (currents, water column temperature and salinity structure, trophic interactions, etc.), making it more relevant to an ecological and hypothesis driven study; however, it demonstrates a potential use of these methods.

Comparison of school thickness with calibrated acoustics

Spatial metrics describing the dimensionality of schools (e.g., area, volume) tend to correlate positively with fish abundance and biomass (Misund et al. 1995). Mean volume backscattering strength (MVBS) also demonstrates similar positive correlation and is often used as a proxy representing abundance or biomass (MacLennan 1990). To validate our school thickness variable, we compared it directly with MVBS, as abundance was

unknown and deriving it from MVBS would introduce additional uncertainty into the comparison. We analyzed three acoustic surveys of the same artificial reef site that were independently conducted using a calibrated split-beam echosounder. This data were not collected simultaneously with MBES data. This allowed split-beam MVBS measurements (Table 1) to be compared with our two variations for calculating school thickness from the same data set. Because split-beam echosounders only collect data along-track (two dimensional), the derivation of school thickness for split-beam data was conducted at the level of 1 m intervals, whereas the resolution of MBES data was at the level of 1×1 m grid cells.

The three split-beam surveys were conducted separate to the MBES surveys, from a 6 m vessel traveling at 2.5 m s^{-1} with a Simrad EK80 echosounder and a 38/200 kHz Combi C transducer mounted over the gunwale (Kongsberg Maritime AS, Horten, Norway). Transmitted pulse length was set to 0.512 ms with transmission power of 500 W and sampling frequency of 15.6 Hz. Prior to each survey, the echosounder was calibrated using standardized methods with a 38.1 mm tungsten carbide sphere (Foote and MacLennan 1984). These split-beam surveys were conducted on 03 December 2018, 01 October 2019, and 25 February 2020, imaging 68 distinct fish schools in total. The difference method and sum method were examined on the 38 kHz wideband (34–45 kHz) data obtained from the EK80 so that we could examine correlation between school thickness and MVBS.

A slightly different approach was necessary to process this two-dimensional split-beam data to extract georeferenced samples (Fig. 1). Data were cleaned to remove background noise, impulse noise, and transient noise prior to echo integration following the methods of De Robertis and Higginbottom (2007) and Ryan et al. (2015) through built-in functions in Echoview (Step S1; Fig. 1). A bottom detection line was generated using Echoview's built-in algorithm and was manually corrected for errors (Step S2). This line was offset by 1 m to exclude any potential bottom backscatter (Ona and Mitson 1996). All data below this line were excluded, as well as all data above a surface line at 6 m depth (Step S3). Schools detection was then performed (Step S4) using the SHAPES algorithm (Fernandes 2009) implemented within the schools detection tool to generate polygon boundaries around distinct schools using a set of schools detection parameters (Supporting Information Table S1) and a detection threshold of −65 dB (Brandt 1996; Loures and Pompeu 2015). For each isolated school, georeferenced samples along with mean volume backscatter for each 1 m interval along the school length were isolated (Step S5) and exported to R (Step S6) where data was visually inspected by plotting in two dimensions.

Although the SHAPES algorithm already provided a measure of school thickness, similar to our difference method, we chose to calculate it ourselves to ensure consistency with our multibeam methods. The two-dimensional data from both school thickness methods was projected to UTM (Step S7) and
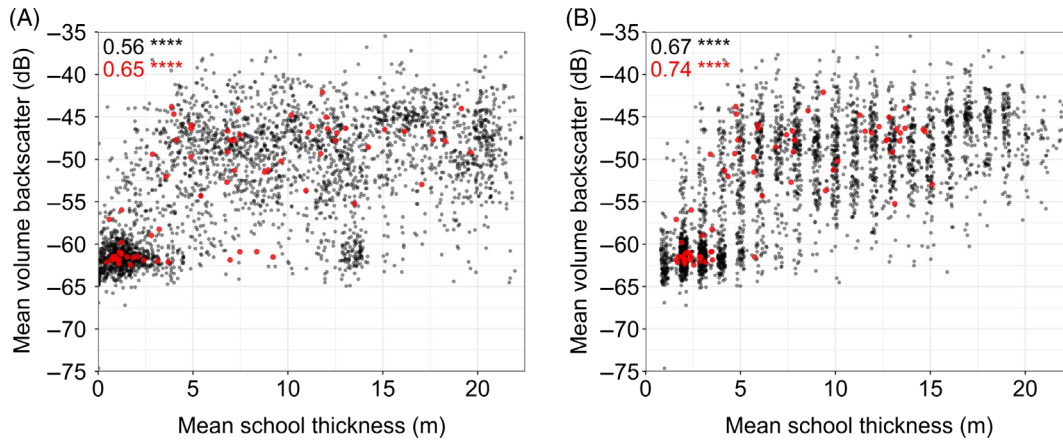
Fig 6. Correlation of mean volume backscatter (dB re 1 m^{-1}) with mean school thickness (split-beam data), with school thickness calculated using the difference method (**a**) or the sum method (**b**). Black points indicate samples at the scale of 1 m intervals and red points indicate the mean values for each of the two variables aggregated at the level of individual schools. Correlation coefficient (*R*) and level of statistical significance are indicated in the top left of each plot, with corresponding colors to the plotted data. Note that in (**b**), x-axis positions are jittered to aid visual interpretation.
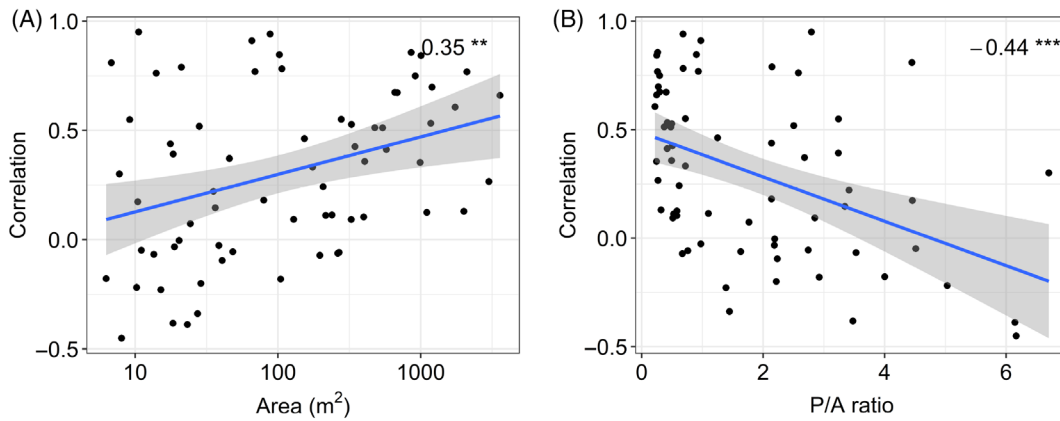
Fig 7. Plots representing the correlation coefficients for school thickness and backscatter at the level of individual schools generated from the sum method, with (**a**) school profile area; and (**b**) school profile perimeter : area ratio. Correlation coefficient (*R*) and level of statistical significance are indicated in the top right of each plot. Linear regression line (blue) and 95% confidence interval (gray) are also displayed.

binned into 1 m intervals (Step S8) so that school thickness could be calculated, as above (Step S9). School thickness was assessed at two scales, which included binning into 1 m intervals and aggregating binned data at the level of individuals schools, by calculating mean school thickness and mean volume backscatter, after conversion to the linear domain.

Pearson correlation tests were conducted for each of the two scales for each method using the "cor.test" function from the stats package. We then conducted paired *t*-tests on the correlation coefficients using the "paired.r" function from the psych package (Revelle 2020) to determine which method demonstrated the best correlation with MVBS.

As the sum method demonstrated stronger positive correlation with MVBS (*see* "Assessment" section), it was then further

examined to determine which characteristics of schools lead to better correlation between school thickness and MVBS. These characteristics included school profile area and perimeter-to-area ratio, which we compared with the correlation coefficients for each of the schools to determine which affected the reliability of our spatial variable.

Assessment

Comparison of school thickness with calibrated acoustics

Comparison of the difference and sum methods

Based on the EK80 split-beam data set, the difference method applied at the scale of 1 m intervals demonstrated a moderate correlation with mean volume backscatter (*R* = 0.56,

p < 0.0001; Fig. 6a); however, correlation was higher for the sum method at this fine scale (*R* = 0.67, *p* < 0.0001; Fig. 6b).

When data were aggregated to the level of individual schools, mean volume backscatter ranged from −62.5 to −42.1 dB. There was higher correlation with school thickness at the level of individual schools than at the level of 1 m intervals for both the difference method (*R* = 0.65, *p* < 0.0001) and the sum method (*R* = 0.74, *p* < 0.0001; Fig. 6).

Paired *t*-tests of the difference between the two dependent correlations indicate that the sum method had higher correlation with backscatter than the difference method at the level of 1 m samples (df = 3093, *t* = −17.23, *p* < 0.0001) and at the level of individual schools (df = 65, *t* = −2.46, *p* = 0.02). Due to its higher correlation with backscatter at both scales, the sum method was selected as a more appropriate method for all further analysis.

Correlation of school thickness and MVBS with variation in school shape

Based on the sum method, correlation coefficients of school thickness with volume backscatter, at the scale of 1 m intervals, were compared to two aspects of school dimensionality, school size (area of the profile), and diffuseness (perimeter to area ratio of the profile) to determine whether these characteristics affected the reliability of our method (Supporting Information Figs. S4, S5). Although the data were not well organized, the total area contained within school profiles was positively correlated with these correlation coefficients for individual schools (*R* = 0.35, *p* < 0.01; Fig. 6a). This result suggests that larger schools are more easily resolved by our method.

Despite high variability in the data, perimeter to area ratio negatively correlated with correlation coefficients (*R* = −0.44, *p* < 0.001; Fig. 7b) suggesting more dispersed and complex school shapes are more difficult to resolve or quantify with our method. Larger areas tend to have lower perimeter to area ratios, so perimeter to area ratio is probably a more appropriate metric for comparing schools in this case. These findings suggest our method should perform best for larger schools with compact boundaries and an approximately elliptical shape, as ellipses exhibit smaller perimeter to area ratio than other shapes with comparative dimensions.

Modeling school distribution around an artificial reef

Remote camera results

Remote video camera footage from each MBES sampling occasion showed the mid-water artificial reef fish community to be dominated by yellowtail scad (*Trachurus novaezelandiae*, 71% of total community abundance) and Australian mado (*Atypichthys strigatus*, 28%). Three other schooling taxa that were observed, silver sweep (*Scorpis lineolata*), one-spot puller (*Chromis hypsilepis*) and silver trevally (*Pseudocaranx georgianus*), but these contributed less than 1% of observed total abundance.
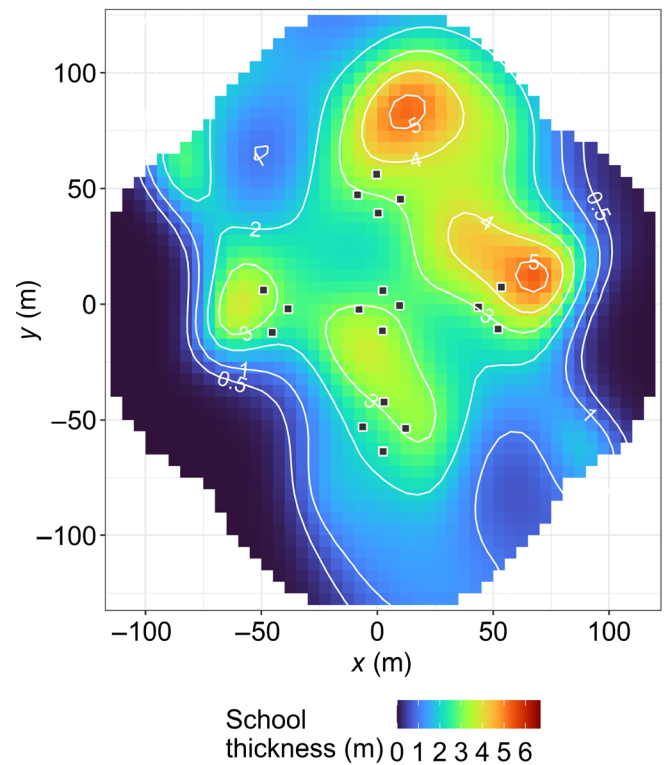

Fig 8. GAMM prediction for the mean distribution of school thickness around the artificial reef. Black squares indicate the locations of the concrete reef modules.

Spatial model results

Our school thickness distribution model explained 18.8% of residual deviance in the absence of random effects (Fig. 8) and a moderate degree of standard error throughout (mean SE = 1.8 m) (Supporting Information Fig. S6). Mean predicted school thickness ranged from 3.0, within 5 m of the nearest reef module, to 0.8, between 65 and 70 m from the nearest reef module. Our GAMM indicated that when summed, 84% of mean school thickness occurred within 50 m of the nearest module. This finding agrees with other studies of the distribution of fish around artificial reefs in the same region (Scott et al. 2015; Smith et al. 2017; Becker et al. 2019).

Overall, our model had limited predictive power (deviance explained: 18.8%), relative to that generated from drop cameras in a similar study (deviance explained: 40.1–66.6%, Becker et al. 2019). This relatively low explained deviance is probably due to large variation in the distribution of fish schools among days, which can be evaluated by exploring each survey's data (Supporting Information Fig. S1). The high proportions of school thickness occurring within 50 m of modules suggest that we likely captured most of the fish schools associated with the reef field. The lower performance than Becker et al. (2019) may also be due to differences in model structure, as Becker et al. (2019) explained relative fish

abundance as a function of bearing to, and distance from, the nearest reef (rather than a function of geographic location).

Discussion

Rapid spatial sampling and estimation of fish distribution across shallow coastal reefs is of critical importance as we increase pressure on our coastal environments (McClanahan et al. 2014; Caldwell et al. 2016). Here we show that a consumer-grade MBES was effective in modeling the distribution of schooling fish around an artificial reef and was able to delineate ecologically meaningful peaks and boundaries in the distribution of fish schools around the reef field. The general patterns measured were similar to those predicted by models produced from drop-cameras (Smith et al. 2017; Becker et al. 2019), a more labor-intensive method that poorly integrates vertical information. Our approach using a relatively low-cost and portable MBES demonstrates that these instruments can provide useful quantitative information on fish distribution, despite their inability to be easily calibrated.

Overall, our results highlight the potential value to coastal ecologists of simple, spatial metrics produced from the new generation of consumer-grade MBES. Although these spatial metrics and MBES are by no means new (Reid and Simmonds 1993; Theberge and Cherkis 2013), the application of nonscientific MBES to marine spatial ecology has been limited. Extraction of three-dimensional targets based on a threshold dB value and subsequently projecting their vertical distribution onto a grid represents a novel approach for working with this large, uncalibrated, and often noisy data to address quantitative ecological questions. While the three-dimensional visualizations generated by MBES can be useful for interpretation, depth-aggregation into a two-dimensional grid of school thickness facilitates spatial calculations and statistical approaches that would otherwise be computationally impractical.

This approach can facilitate the detection of consistent patterns in distribution. Our fitted GAMM indicated that the greatest peaks in school thickness may not occur in the immediate vicinity of reef modules. Rather, school thickness was generally concentrated to the northeast of both the northern and the eastern module cluster. Since the three-dimensional module outlines were excluded from the acoustic data before samples were exported (Fig. 3), it is unlikely that peaks were driven by the modules themselves. The fact that peaks in school thickness were offset with the same relative distance and bearing from module clusters, rather than centered around module clusters is ecologically meaningful, suggesting that fish consistently assemble along the northeast (offshore) side of the reef structure to feed in the predominant southwesterly current. The artificial reef field was designed with this specific module placement so that the provision of fish habitat would be greater than the sum of the individual modules. These observations are important because they highlight an association between schooling fish and benthic structure that would not have been well resolved by alternate survey methods.

Applying acoustic techniques to monitor fine-scale distribution of multispecies assemblages around benthic structure, such as reefs, still presents significant challenges (Boswell et al. 2020), as it is common for multiple species to forage together in the water column (Lukoschek and McCormick 2000). This school heterogeneity significantly complicates traditional fisheries acoustic approaches (Boswell et al. 2020). Although there exists high variability in translating school thickness to actual fish abundance (Zwolinski et al. 2009), the high correlation of this variable with mean volume backscatter from the split-beam echosounder suggests that school thickness can be a useful representation for the relative distribution of schools. As a measure of relative distribution, it is not that dissimilar to more common methods for deriving relative abundance, such as MaxN from remote video count data (Schobernd et al. 2014; Campbell et al. 2015), from which absolute abundance is unknown but expected to scale relatively.

Due to the spatially continuous nature and high resolution associated with MBES data, it is possible that models of the mean fish distribution generated using our method will also have lower predictive power than those produced from point data, such as underwater video (Saveliev et al. 2007; Li and Heap 2011). However, to achieve a similar outcome using underwater video methods is substantially more laborious. Becker et al. (2019) predicted the distribution of fish around an artificial reef by saturating a similarly designed reef field with 40 drop camera deployments of 2 min duration each over 24 d, resulting in 960 deployments and 32 h of footage. By comparison, we conducted only five MBES surveys of 40 min duration at our site, which took 3.33 h in total. Like Becker et al. (2019), we also observed a sharp decline in fish density with increasing distance from the nearest module, as has been documented in other studies of artificial reefs (Boswell et al. 2010; Champion et al. 2015). This pattern, known as the thigmotaxic response, or the tendency for animals to move toward structure rather than bare habitat, is a dominant process structuring the distribution of fishes (Brickhill et al. 2005; Sheehan et al. 2020), even when it acts to their detriment (Hallier and Gaertner 2008). In the context of artificial reefs, this process is the basis for the enduring "fish attraction" debate (Bohnsack 1989; Pickering and Whitmarsh 1997; Smith et al. 2015).

Despite the strong attraction of fish to the reef structure, fish schools will relocate among surveys, and even redistribute over the course of a single survey. Due to the non-instantaneous nature of data acquisition, this redistribution is an important consideration for acoustic surveys, as it is for underwater visual census and video methods (Schobernd et al. 2014). At the finest scale, this may lead to aliasing of individual targets (Colbo et al. 2014), although our grid-based

averaging approach should reduce this effect. At a coarser scale, redistribution could cause some schools to be surveyed multiple times and some to remain unsurveyed. This potential source of error should be diminished in the vicinity of large reefs, as many schooling fish maintain close proximity to structure (Szedlmayer and Schroepfer 2005; Lowry et al. 2017) and can demonstrate high site fidelity, even within multi-reef arrays (Taylor et al. 2018). Depending on the site and the dynamics of the fish species under investigation, to obtain adequate survey coverage and improve data quality it may be necessary to conduct overlapping parallel transects or to conduct transects from multiple directions to overcome issues of shadowing behind seafloor features. Nevertheless, a robust sampling design would initially evaluate variation in the abundance of fish schools and their distribution, to ensure sufficient surveys are done to estimate metrics of interest (such as the mean distribution).

A major advantage of MBES is that they can fully capture the spatial boundaries of schools and habitat features across all three dimensions. As school thickness indicates the height of a school across a grid, school volume can be accurately estimated and volume estimates can be used to calculate abundance, presuming there is knowledge of density within the school. In addition to this school thickness variable we derived, there are additional gridded spatial variables pertaining to school distribution which would be straightforward to generate with only minor modifications to our rasterization methods. The simultaneous high-resolution measurement of water column and seafloor data produced by MBES makes them particularly well suited for studying the spatial distribution of fish relative to their habitat. A good example of this is "height above bottom," or simply the vertical distance between the fish in a grid cell and the seafloor (Weber et al. 2009). This variable can indicate how strongly schooling fish associate with the seafloor (Holzman et al. 2007). It would be similarly easy to apply these methods to studying the depth of fish relative to the water surface. This could be useful in studying vessel avoidance (Vabø et al. 2002) or the response of schooling fish to the threat of surface predators, such as seabirds (Fauchald 2009).

We demonstrated our method for processing and summarizing MBES data by mapping the depth-aggregated distribution of fish around a nearshore artificial reef, but this approach could be readily adapted to other applications concerning the distribution of schooling fish around benthic structures, such as sewage outfalls (Grigg 1994) and subsea pipelines associated with the oil and gas industry (Bond et al. 2018). These artificial habitats present linear sources of structure (rather than point sources, as in our case) which may be used by schooling fish in a similar way to artificial reefs (Love and York 2005; McLean et al. 2017). Typical approaches to monitoring pipelines have involved the use of manned submersibles (Love and York 2005), remote operated vehicles (ROV) (McLean et al. 2017), and baited remote underwater

video (BRUV) (Bond et al. 2018), which provide species-level abundance data and, with stereo methods, can be used to estimate fish biomass. However, for more routine monitoring of fish distribution around these structures, MBES and summary metrics such as school thickness are likely to be more efficient. An additional benefit is that MBES do not affect fish behavior in the way that manned-submersible, ROV, and BRUV methods can (Schramm et al. 2020). Although echosounders cannot match the species-level detail provided by underwater video, the superior survey efficiency provided by MBES could be used to increase the frequency of surveys for applications where high temporal resolution is necessary.

References

Basford, A. J., D. A. Feary, G. Truong, P. D. Steinberg, E. M. Marzinelli, and A. Vergés. 2016. Feeding habits of range-shifting herbivores: Tropical surgeonfishes in a temperate environment. Mar. Freshw. Res. **67**: 75–83. doi:10.1071/MF14208

Becker, A., M. Holland, J. A. Smith, and I. M. Suthers. 2016. Fish movement through an estuary mouth is related to tidal flow. Estuaries Coast. **39**: 1199–1207. doi:10.1007/s12237-015-0043-3

Becker, A., J. A. Smith, M. D. Taylor, J. McLeod, and M. B. Lowry. 2019. Distribution of pelagic and epi-benthic fish around a multi-module artificial reef-field: Close module spacing supports a connected assemblage. Fish. Res. **209**: 75–85. doi:10.1016/j.fishres.2018.09.020

Bellwood, D. R., R. P. Streit, S. J. Brandl, and S. B. Tebbett. 2019. The meaning of the term 'function' in ecology: A coral reef perspective. Funct. Ecol. **33**: 948–961. doi:10.1111/1365-2435.13265

Bohnsack, J. A. 1989. Are high densities of fishes at artificial reefs the result of habitat limitation or behavioral preference? Bull. Mar. Sci. **44**: 631–645. Available from https://www.ingentaconnect.com/contentone/umrsmas/bullmar/1989/00000044/00000002/art00009.

Bond, T., J. C. Partridge, M. D. Taylor, T. F. Cooper, and D. L. McLean. 2018. The influence of depth and a subsea pipeline on fish assemblages and commercially fished species. PLoS One **13**: e0207703. doi:10.1371/journal.pone.0207703

Boswell, K. M., R. Wells, J. H. Cowan Jr., and C. A. Wilson. 2010. Biomass, density, and size distributions of fishes associated with a large-scale artificial reef complex in the Gulf of Mexico. Bull. Mar. Sci. **86**: 879–889. doi:10.5343/bms.2010.1026

Boswell, K. M., G. Pedersen, J. C. Taylor, S. LaBua, and W. F. Patterson III. 2020. Examining the relationship between morphological variation and modeled broadband scattering responses of reef-associated fishes from the Southeast United States. Fish. Res. **228**: 105590. doi:10.1016/j.fishres.2020.105590

Brandt, S. 1996. Acoustic assessment of fish abundance and distribution, p. 385–432. *In* Murphy Brian R., and Willis David W. Fisheries techniques, 2nd ed. American Fisheries Society.

Brickhill, M., S. Lee, and R. Connolly. 2005. Fishes associated with artificial reefs: Attributing changes to attraction or production using novel approaches. J. Fish Biol. **67**: 53–71. doi:10.1111/j.0022-1112.2005.00915.x

Caldwell, Z. R., B. J. Zgliczynski, G. J. Williams, and S. A. Sandin. 2016. Reef fish survey techniques: Assessing the potential for standardizing methodologies. PLoS One **11**: e0153066. doi:10.1371/journal.pone.0153066

Campbell, M. D., A. G. Pollack, C. T. Gledhill, T. S. Switzer, and D. A. DeVries. 2015. Comparison of relative abundance indices calculated from two methods of generating video count data. Fish. Res. **170**: 125–133. doi:10.1016/j.fishres.2015.05.011

Champion, C., I. M. Suthers, and J. A. Smith. 2015. Zooplanktivory is a key process for fish production on a coastal artificial reef. Mar. Ecol. Prog. Ser. **541**: 1–14. doi:10.3354/meps11529

Claisse, J. T., D. J. Pondella, M. Love, L. A. Zahn, C. M. Williams, J. P. Williams, and A. S. Bull. 2014. Oil platforms off California are among the most productive marine fish habitats globally. Proc. Natl. Acad. Sci. USA **111**: 15462–15467. doi:10.1073/pnas.1411477111

Clarke, J. H. 2006. Applications of multibeam water column imaging for hydrographic survey. Hydrogr. J. **120**: 3. Available from http://citeseerx.ist.psu.edu/viewdoc/download?doi=10.1.1.452.3020&rep=rep1&type=pdf.

Colbo, K., T. Ross, C. Brown, and T. Weber. 2014. A review of oceanographic applications of water column data from multibeam echosounders. Estuar. Coast. Shelf Sci. **145**: 41–56. doi:10.1016/j.ecss.2014.04.002

De Robertis, A., and I. Higginbottom. 2007. A post-processing technique to estimate the signal-to-noise ratio and remove echosounder background noise. ICES J. Mar. Sci. **64**: 1282–1291. doi:10.1093/icesjms/fsm112

Denney, C., Fields, R., Gleason, M., and Starr, R. 2017. Development of New Methods for Quantifying Fish Density Using Underwater Stereo-video Tools. J. Vis. Exp. (129). doi:10.3791/56635

Dickens, L. C., C. H. Goatley, J. K. Tanner, and D. R. Bellwood. 2011. Quantifying relative diver effects in underwater visual censuses. PLoS One **6**: e18965. doi:10.1371/journal.pone.0018965

Dix, M., A. Abd-Elrahman, B. Dewitt, and L. Nash Jr. 2012. Accuracy evaluation of terrestrial LiDAR and multibeam sonar systems mounted on a survey vessel. J. Surv. Eng. **138**: 203–213. doi:10.1061/(ASCE)SU.1943-5428.0000075

dos Santos, L. N., D. S. Brotto, and I. R. Zalmon. 2010. Fish responses to increasing distance from artificial reefs on the Southeastern Brazilian Coast. J. Exp. Mar. Biol. Ecol. **386**: 54–60. doi:10.1016/j.jembe.2010.01.018

Dougherty, E. R. 1992. An introduction to morphological image processing, v. **1992**. SPIE.

Edgar, G. J., N. S. Barrett, and A. J. Morton. 2004. Biases associated with the use of underwater visual census techniques to quantify the density and size-structure of fish populations. J. Exp. Mar. Biol. Ecol. **308**: 269–290. doi:10.1016/j.jembe.2004.03.004

Egerton Jack P., G. Bolser Derek, Grüss Arnaud, and E. Erisman Brad. 2021. Understanding patterns of fish backscatter, size and density around petroleum platforms of the U.S. Gulf of Mexico using hydroacoustic data. Fish. Res. **233**: 105752. doi:10.1016/j.fishres.2020.105752.

Ellis, D., and E. E. DeMartini. 1995. Evaluation of video camera technique for indexing abundances of juvenile pink snapper *Pristipomoides filamentosus*, and other Hawaiian insular shelf fishes. Fish. Bull. **93**: 67–77. Available from https://ci.nii.ac.jp/naid/10004871220/.

Fauchald, P. 2009. Spatial interaction between seabirds and prey: Review and synthesis. Mar. Ecol. Prog. Ser. **391**: 139–151. doi:10.3354/meps07818

Fernandes, P. G. 2009. Classification trees for species identification of fish-school echotraces. ICES J. Mar. Sci. **66**: 1073–1080. doi:10.1093/icesjms/fsp060

Folpp, H., Lowry, M., Gregson, M., and Suthers, I. M. 2011. Colonization and community development of fish assemblages associated with estuarine artificial reefs. Braz. J. Oceanogr. **59**(spe1):55–67. doi:10.1590/s1679-87592011000500008.

Foote, K. G., and D. N. MacLennan. 1984. Comparison of copper and tungsten carbide calibration spheres. J. Acoust. Soc. Am. **75**: 612–616. doi:10.1121/1.390489

Foote, K. G., D. Chu, T. R. Hammar, K. C. Baldwin, L. A. Mayer, L. C. Hufnagle Jr., and J. M. Jech. 2005. Protocols for calibrating multibeam sonar. J. Acoust. Soc. Am. **117**: 2013–2027. doi:10.1121/1.1869073

Fréon, P., F. Gerlotto, and M. Soria. 1992. Changes in school structure according to external stimuli: Description and influence on acoustic assessment. Fish. Res. **15**: 45–66. doi:10.1016/0165-7836(92)90004-D

Graham, N., and K. Nash. 2013. The importance of structural complexity in coral reef ecosystems. Coral Reefs **32**: 315–326. doi:10.1007/s00338-012-0984-y

Grigg, R. W. 1994. Effects of sewage discharge, fishing pressure and habitat complexity on coral ecosystems and reef fishes in Hawaii. Mar. Ecol. Prog. Ser. **103**: 25–34. doi:10.3354/meps103025

Guillard, J., F. Paul, T. Laloë, and P. Brehmer. 2011. Three-dimensional internal spatial structure of young-of-the-year pelagic freshwater fish provides evidence for the identification of fish school species. Limnol. Oceanogr.: Methods **9**: 322–328. doi:10.4319/lom.2011.9.322

Hallier, J.-P., and D. Gaertner. 2008. Drifting fish aggregation devices could act as an ecological trap for tropical tuna species. Mar. Ecol. Prog. Ser. **353**: 255–264. doi:10.3354/meps07180

Hamner, W., M. Jones, J. Carleton, I. Hauri, and D. M. Williams. 1988. Zooplankton, planktivorous fish, and water currents on a windward reef face: Great Barrier Reef, Australia. Bull. Mar. Sci. **42**: 459–479. Available from https://www.ingentaconnect.com/contentone/umrsmas/bullmar/1988/00000042/00000003/art00010.

Harvey, E., D. Fletcher, M. R. Shortis, and G. A. Kendrick. 2004. A comparison of underwater visual distance estimates made by scuba divers and a stereo-video system: Implications for underwater visual census of reef fish abundance. Mar. Freshw. Res. **55**: 573–580. doi:10.1071/MF03130

Hijmans, R. J., and others. 2015. Package 'raster'. R package.

Holland, M. M., J. A. Smith, J. D. Everett, A. Vergés, and I. M. Suthers. 2020. Latitudinal patterns in trophic structure of temperate reef-associated fishes and predicted consequences of climate change. Fish Fish. **21**: 1092–1108. doi:10.1111/faf.12488

Holzman, R., M. Ohavia, R. Vaknin, and A. Genin. 2007. Abundance and distribution of nocturnal fishes over a coral reef during the night. Mar. Ecol. Prog. Ser. **342**: 205–215. doi:10.3354/meps342205

Hunter, W., and M. Sayer. 2009. The comparative effects of habitat complexity on faunal assemblages of northern temperate artificial and natural reefs. ICES J. Mar. Sci. **66**: 691–698. doi:10.1093/icesjms/fsp058

Innangi, S., A. Bonanno, R. Tonielli, F. Gerlotto, M. Innangi, and S. Mazzola. 2016. High resolution 3-D shapes of fish schools: A new method to use the water column backscatter from hydrographic MultiBeam Echo Sounders. Appl. Acoust. **111**: 148–160. doi:10.1016/j.apacoust.2016.04.017

Jung, D., J. Kim, and G. Byun. 2018. Numerical modeling and simulation technique in time-domain for multibeam echo sounder. Int. J. Naval Archit. Ocean Eng. **10**: 225–234. doi:10.1016/j.ijnaoe.2017.08.004

Kang, M.-H. 2011. Semiautomated analysis of data from an imaging sonar for fish counting, sizing, and tracking in a post-processing application. Fish. Aquat. Sci. **14**: 218–225. doi:10.5657/FAS.2011.0218

Kieser, R., T. Mulligan, L. J. Richards, and B. Leaman. 1993. Bias correction of rockfish school cross section widths from digitized echo sounder data. Can. J. Fish. Aquat. Sci. **50**: 1801–1811. doi:10.1139/f93-202

Kuriyama, P. T., J. P. Zwolinski, K. T. Hill, and P. R. Crone. 2020. Assessment of the Pacific sardine resource in 2020 for US management in 2020–2021. doi:10.25923/r2fz-4y79

Lee, D.-J. 2013. Monitoring of fish aggregations responding to artificial reefs using a split-beam echo sounder, side-scan sonar, and an underwater CCTV camera system at Suyeong Man, Busan, Korea. Korean J. Fish. Aquat. Sci. **46**: 266–272. doi:10.5657/KFAS.2013.0266

Leitao, F., M. N. Santos, K. Erzini, and C. C. Monteiro. 2008. Fish assemblages and rapid colonization after enlargement of an artificial reef off the Algarve coast (Southern Portugal). Mar. Ecol. **29**: 435–448. doi:10.1111/j.1439-0485.2008.00253.x

Li, J., and A. D. Heap. 2011. A review of comparative studies of spatial interpolation methods in environmental sciences: Performance and impact factors. Ecol. Inform. **6**: 228–241. doi:10.1016/j.ecoinf.2010.12.003

Loures R. C., and P. S. Pompeu. 2015. Seasonal and diel changes in fish distribution in a tropical hydropower plant tailrace: evidence from hydroacoustic and gillnet sampling. Fish. Manag. Ecol. **22**(3): 185–196. doi:10.1111/fme.12116.

Love, M. S., and A. York. 2005. A comparison of the fish assemblages associated with an oil/gas pipeline and adjacent seafloor in the Santa Barbara Channel, Southern California Bight. Bull. Mar. Sci. **77**: 101–118. Available from https://www.ingentaconnect.com/contentone/umrsmas/bullmar/2005/00000077/00000001/art00007.

Lowry, M., T. Glasby, C. Boys, H. Folpp, I. Suthers, and M. Gregson. 2014. Response of fish communities to the deployment of estuarine artificial reefs for fisheries enhancement. Fish. Manag. Ecol. **21**: 42–56. doi:10.1111/fme.12048

Lowry, M., A. Becker, H. Folpp, J. McLeod, and M. D. Taylor. 2017. Residency and movement patterns of yellowfin bream (*Acanthopagrus australis*) released at natural and artificial reef sites. Mar. Freshw. Res. **68**: 1479–1488. doi:10.1071/MF16351

Lukoschek, V., and M. McCormick. 2000. A review of multispecies foraging associations in fishes and their ecological significance. *In* Paper presented at the Proceedings of the 9th International Coral Reef Symposium.

MacLennan David N. 1990. Acoustical measurement of fish abundance. J. Acoust. Soc. Am. **87**(1): 1–15. doi:10.1121/1.399285.

MacNeil, M. A., E. H. Tyler, C. J. Fonnesbeck, S. P. Rushton, N. V. Polunin, and M. J. Conroy. 2008. Accounting for detectability in reef-fish biodiversity estimates. Mar. Ecol. Prog. Ser. **367**: 249–260. doi:10.3354/meps07580

Mayer, L., Y. Li, and G. Melvin. 2002. 3D visualization for pelagic fisheries research and assessment. ICES J. Mar. Sci. **59**: 216–225. doi:10.1006/jmsc.2001.1125

McClanahan, T. R., N. A. Graham, and E. S. Darling. 2014. Coral reefs in a crystal ball: Predicting the future from the vulnerability of corals and reef fishes to multiple stressors. Curr. Opin. Environ. Sustain. **7**: 59–64. doi:10.1016/j.cosust.2013.11.028

McLean, D., J. Partridge, T. Bond, M. Birt, K. Bornt, and T. Langlois. 2017. Using industry ROV videos to assess fish associations with subsea pipelines. Cont. Shelf Res. **141**: 76–97. doi:10.1016/j.csr.2017.05.006

McLean, D., M. Taylor, A. G. Ospina, and J. Partridge. 2019. An assessment of fish and marine growth associated with an oil and gas platform jacket using an augmented remotely operated vehicle. Cont. Shelf Res. **179**: 66–84. doi:10.1016/j.csr.2019.04.006

Misund, O. A., A. Aglen, and E. Frønæs. 1995. Mapping the shape, size, and density of fish schools by echo integration and a high-resolution sonar. ICES J. Mar. Sci. **52**: 11–20. doi:10.1016/1054-3139(95)80011-5

Monk, J., D. Ierodiaconou, V. L. Versace, A. Bellgrove, E. Harvey, A. Rattray, L. Laurenson, and G. P. Quinn. 2010. Habitat suitability for marine fishes using presence-only modelling and multibeam sonar. Mar. Ecol. Prog. Ser. **420**: 157–174. doi:10.3354/meps08858

Monk, J., D. Ierodiaconou, E. Harvey, A. Rattray, and V. L. Versace. 2012. Are we predicting the actual or apparent distribution of temperate marine fishes? PLoS One **7**: e34558. doi:10.1371/journal.pone.0034558

Morais, R. A., and D. R. Bellwood. 2019. Pelagic subsidies underpin fish productivity on a degraded coral reef. Curr. Biol. **29**: 1521–1527. doi:10.1016/j.cub.2019.03.044

Murdoch, D. 2001. RGL: An R interface to OpenGL. *In* Paper presented at the Proceedings of DSC.

Murphy Hannah M., and P. Jenkins Gregory. 2010. Observational methods used in marine spatial monitoring of fishes and associated habitats: a review. Mar. Freshwater Res. **61** (2): 236. doi:10.1071/mf09068.

O'Donnell, C., E. Mullins, D. Lynch, K. Lyons, P. 2019. Connaughton, and J. Power. 2019. Celtic Sea herring acoustic survey cruise report. 9–29 October 2019. Available from https://oar.marine.ie/handle/10793/1494. (Accessed 12 September 2020).

Ona, E., and R. Mitson. 1996. Acoustic sampling and signal processing near the seabed: The deadzone revisited. ICES J. Mar. Sci. **53**: 677–690. doi:10.1006/jmsc.1996.0087

Paramo, J., S. Bertrand, H. Villalobos, and F. Gerlotto. 2007. A three-dimensional approach to school typology using vertical scanning multibeam sonar. Fish. Res. **84**: 171–179. doi:10.1016/j.fishres.2006.10.023

Parsons, D. F., I. M. Suthers, D. O. Cruz, and J. A. Smith. 2016. Effects of habitat on fish abundance and species composition on temperate rocky reefs. Mar. Ecol. Prog. Ser. **561**: 155–171. doi:10.3354/meps11927

Paxton, A. B., J. C. Taylor, C. Peterson, S. R. Fegley, and J. H. Rosman. 2019. Consistent spatial patterns in multiple trophic levels occur around artificial habitats. Mar. Ecol. Prog. Ser. **611**: 189–202. doi:10.3354/meps12865

Pickering, H., and D. Whitmarsh. 1997. Artificial reefs and fisheries exploitation: A review of the 'attraction versus production' debate, the influence of design and its significance for policy. Fish. Res. **31**: 39–59. doi:10.1016/S0165-7836(97)00019-2

Punzo, E., S. Malaspina, F. Domenichetti, P. Polidori, G. Scarcella, and G. Fabi. 2015. Fish detection around offshore artificial structures: Preliminary results from hydroacoustics and fishing surveys. J. Appl. Ichthyol. **31**: 48–59. doi:10.1111/jai.12950

R Core Team. 2018. R: A language and environment for statistical computing (Version 3.5.1).

Reid, D., and E. Simmonds. 1993. Image analysis techniques for the study of fish school structure from acoustic survey data. Can. J. Fish. Aquat. Sci. **50**: 886–893. doi:10.1139/f93-102

Revelle, W. 2020. psych: Procedures for personality and psychological research. R package version 2.0.8. Available from https://CRAN.R-project.org/package=psych

Rieucau, G., K. M. Boswell, M. E. Kimball, G. Diaz, and D. M. Allen. 2015. Tidal and diel variations in abundance and schooling behavior of estuarine fish within an intertidal salt marsh pool. Hydrobiologia **753**: 149–162. doi:10.1007/s10750-015-2202-8

Rilov, G., and Y. Benayahu. 1998. Vertical artificial structures as an alternative habitat for coral reef fishes in disturbed environments. Mar. Environ. Res. **45**: 431–451. doi:10.1016/S0141-1136(98)00106-8

Roche, M., K. Degrendele, C. Vrignaud, S. Loyer, T. Le Bas, J.-M. Augustin, and X. Lurton. 2018. Control of the repeatability of high frequency multibeam echosounder backscatter by using natural reference areas. Mar. Geophys. Res. **39**: 89–104. doi:10.1007/s11001-018-9343-x

Rudstam, L. G., S. Hansson, T. Lindem, and D. W. Einhouse. 1999. Comparison of target strength distributions and fish densities obtained with split and single beam echo sounders. Fish. Res. **42**: 207–214. doi:10.1016/S0165-7836(99)00047-8

Ryan, T. E., R. A. Downie, R. J. Kloser, and G. Keith. 2015. Reducing bias due to noise and attenuation in open-ocean echo integration data. ICES J. Mar. Sci. **72**: 2482–2493. doi:10.1093/icesjms/fsv121

Sala, A., G. Fabi, and S. Manoukian. 2007. Vertical diel dynamic of fish assemblage associated with an artificial reef (Northern Adriatic Sea). Sci. Mar. **71**: 355–364. doi:10.3989/scimar.2007.71n2355

Saveliev, A., S. Mukharamova, N. Chizhikova, R. Budgey, and A. and Zuur. 2007. Spatially continuous data analysis and modelling, p. 341–372. *In* Zuur Alain, N. Ieno Elena, and M. Smith Graham [eds.], Analysing ecological data. Springer.

Schoberd, Z. H., N. M. Bacheler, and P. B. Conn. 2014. Examining the utility of alternative video monitoring metrics for indexing reef fish abundance. Can. J. Fish. Aquat. Sci. **71**: 464–471. doi:10.1139/cjfas-2013-0086

Schramm, K. D., E. S. Harvey, J. S. Goetze, M. J. Travers, B. Warnock, and B. J. Saunders. 2020. A comparison of stereo-BRUV, diver operated and remote stereo-video transects for assessing reef fish assemblages. J. Exp. Mar. Biol. Ecol. **524**: 151273. doi:10.1016/j.jembe.2019.151273

Scott, M. E., J. A. Smith, M. B. Lowry, M. D. Taylor, and I. M. Suthers. 2015. The influence of an offshore artificial reef on the abundance of fish in the surrounding pelagic environment. Mar. Freshw. Res. **66**: 429–437. doi:10.1071/MF14064

Sheehan, E. V., D. Bridger, S. J. Nancollas, and S. J. Pittman. 2020. *PelagiCam*: A novel underwater imaging system with

computer vision for semi-automated monitoring of mobile marine fauna at offshore structures. Environ. Monit. Assess. **192**: 11. doi:10.1007/s10661-019-7980-4

Simmonds, J., and MacLennan, D. 2013. Fisheries Acoustics: Theory and Practice, 2nd Edition. Wiley-Blackwell. doi:10.1007/978-94-017-1558-4

Smith, J. A., M. B. Lowry, and I. M. Suthers. 2015. Fish attraction to artificial reefs not always harmful: A simulation study. Ecol. Evol. **5**: 4590–4602. doi:10.1002/ece3.1730

Smith, J. A., M. B. Lowry, C. Champion, and I. M. Suthers. 2016. A designed artificial reef is among the most productive marine fish habitats: New metrics to address 'production versus attraction'. Mar. Biol. **163**: 188. doi:10.1007/s00227-016-2967-y

Smith, J. A., W. K. Cornwell, M. B. Lowry, and I. M. Suthers. 2017. Modelling the distribution of fish around an artificial reef. Mar. Freshw. Res. **68**: 1955–1964. doi:10.1071/MF16019

Soldal, A. V., I. Svellingen, T. Jørgensen, and S. Løkkeborg. 2002. Rigs-to-reefs in the North Sea: Hydroacoustic quantification of fish in the vicinity of a "semi-cold" platform. ICES J. Mar. Sci. **59**: S281–S287. doi:10.1006/jmsc.2002.1279

Szedlmayer, S. T., and R. L. Schroepfer. 2005. Long-term residence of red snapper on artificial reefs in the northeastern Gulf of Mexico. Trans. Am. Fish. Soc. **134**: 315–325. doi:10.1577/T04-070.1

Tassetti, A., S. Malaspina, and G. Fabi. 2015. Using a multibeam echosounder to monitor an artificial reef. Int. Arch. Photogramm. Remote Sens. Spat. Inf. Sci. **XL-5/W5**: 207–213. doi:10.5194/isprsarchives-XL-5-W5-207-2015

Taylor, J., and E. Ebert. 2012. Mapping coral reef fish schools and aggregations with high-frequency multibeam and split-beam sonars. *In* Paper presented at the Proceedings of Meetings on Acoustics ECUA2012.

Taylor, M. D., A. Becker, and M. B. Lowry. 2018. Investigating the functional role of an artificial reef within an estuarine seascape: A case study of yellowfin bream (*Acanthopagrus australis*). Estuaries Coast. **41**: 1782–1792. doi:10.1007/s12237-018-0395-6

Theberge, A. E. J., and N. Z. Cherkis. 2013. A note on fifty years of multi-beam. *Hydro International*, *22*. Available from https://www.hydro-international.com/content/article/a-note-on-fifty-years-of-multi-beam (Accessed 15 September 2020).

Trenkel, V. M., V. Mazauric, and L. Berger. 2008. The new fisheries multibeam echosounder ME70: Description and expected contribution to fisheries research. ICES J. Mar. Sci. **65**: 645–655. doi:10.1093/icesjms/fsn051

Truong, L., I. M. Suthers, D. O. Cruz, and J. A. Smith. 2017. Plankton supports the majority of fish biomass on temperate rocky reefs. Mar. Biol. **164**: 73. doi:10.1007/s00227-017-3101-5

Vabø, R., K. Olsen, and I. Huse. 2002. The effect of vessel avoidance of wintering Norwegian spring spawning herring. Fish. Res. **58**: 59–77. doi:10.1016/S0165-7836(01)00360-5

Watson, D. L., E. S. Harvey, M. J. Anderson, and G. A. Kendrick. 2005. A comparison of temperate reef fish assemblages recorded by three underwater stereo-video techniques. Mar. Biol. **148**: 415–425. doi:10.1007/s00227-005-0090-6

Weber, T. C., H. Peña, and J. M. Jech. 2009. Consecutive acoustic observations of an Atlantic herring school in the Northwest Atlantic. ICES J. Mar. Sci. **66**: 1270–1277. doi:10.1093/icesjms/fsp090

Zwolinski, J., P. G. Fernandes, V. Marques, and Y. Stratoudakis. 2009. Estimating fish abundance from acoustic surveys: Calculating variance due to acoustic backscatter and length distribution error. Can. J. Fish. Aquat. Sci. **66**: 2081–2095. doi:10.1139/F09-138

Conflict of Interest

None declared.